Supplementary Information

2.9 Pharmacophore modelling

Pharmacophore features of the structures of the compounds **1** and **2** were identified using Ligandscout software which also demonstrates significant Structure Activity Relationship (SAR).[1] and optimal molecular interactions with protein targets. The fully optimised structures of the complexes were loaded into Ligandscout software and core pharmacophore features were identified including H-bond donor, H-bond acceptor, hydrophobic, aromatic, halogen-bond donor, positive and negative ionizable groups.[2]

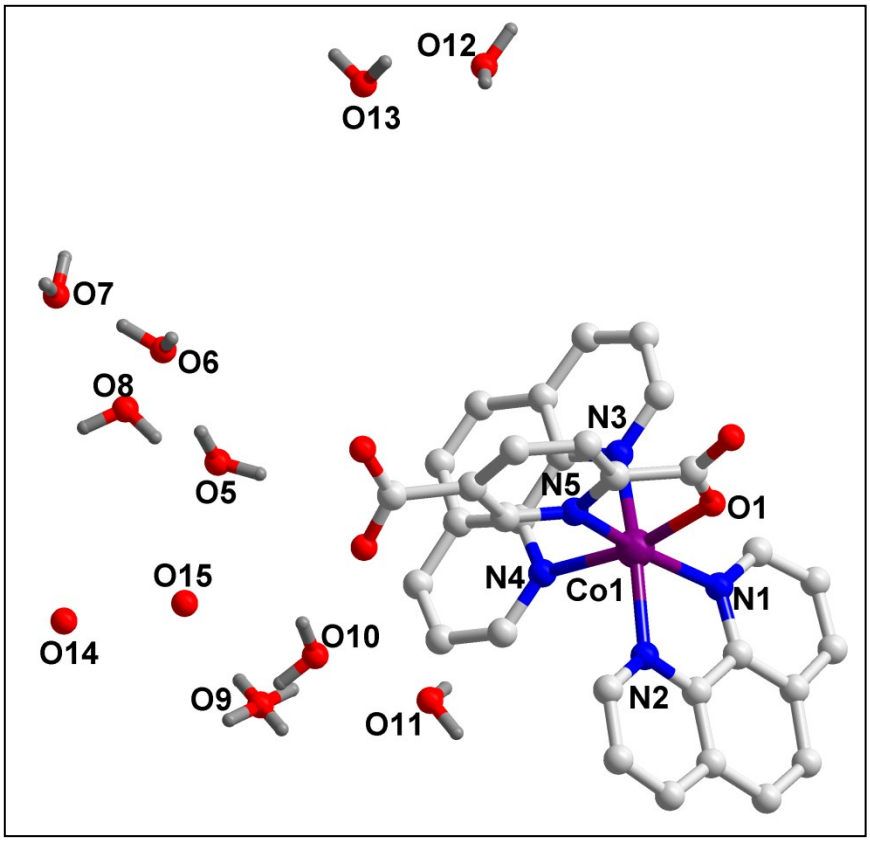

Fig. **S1** Molecular structure of $[Co(2,5\text{-}PDC)(phen)_2]\cdot 9H_2O$ (**1**). Aromatic hydrogen atoms are omitted for clarity.

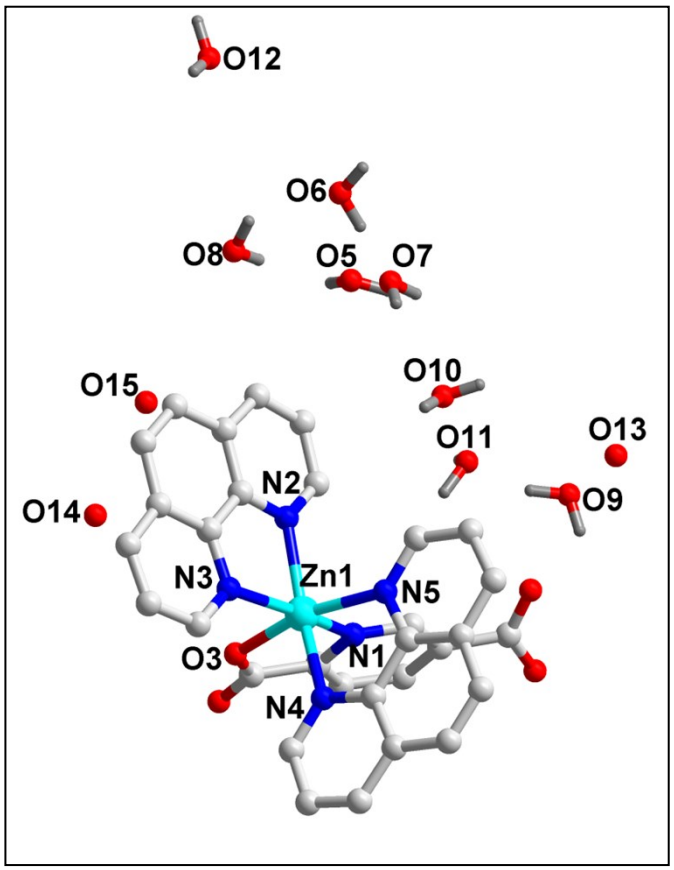

Fig. **S2** Molecular structure of [Zn(2,5-PDC)(phen)$_2$]·9H$_2$O (**2**). Aromatic hydrogen atoms are omitted for clarity.

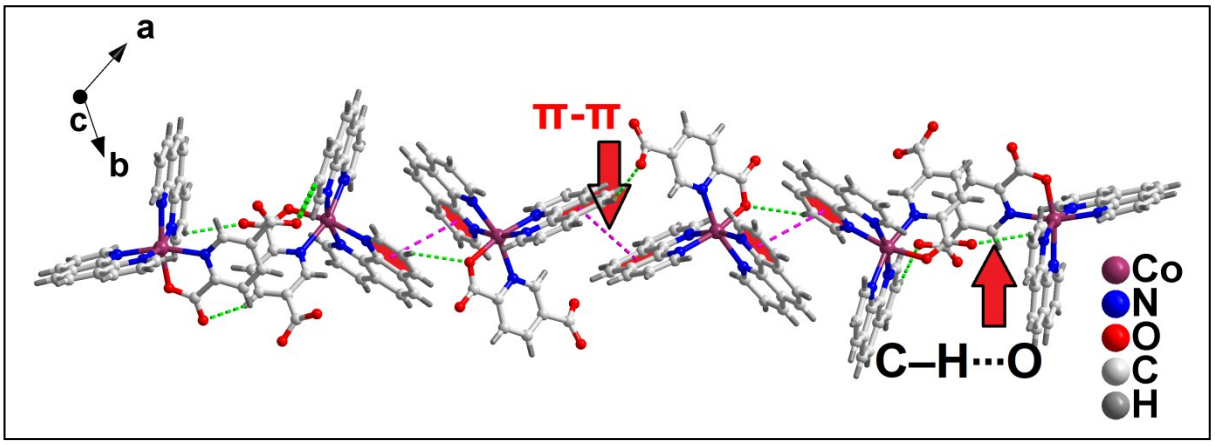

Fig. **S3** 1D supramolecular chain of compound **1** involving π-π stacking and C–H···O hydrogen bonding interactions.

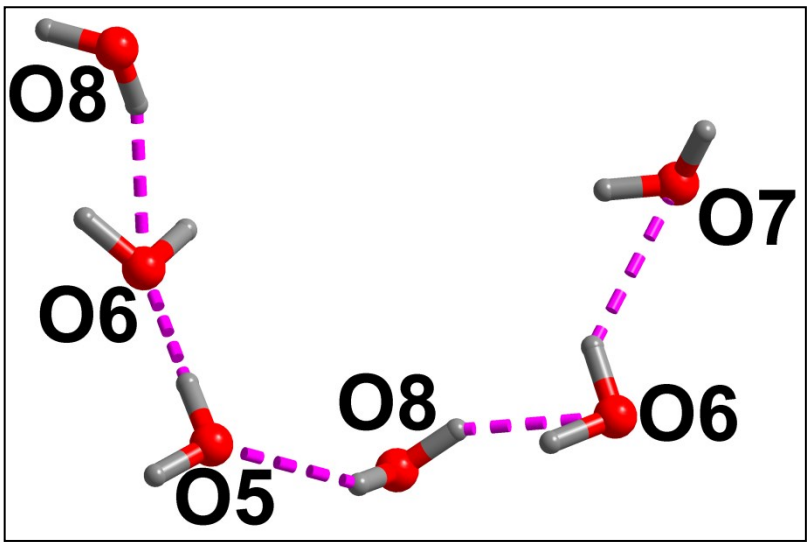

(**a**)

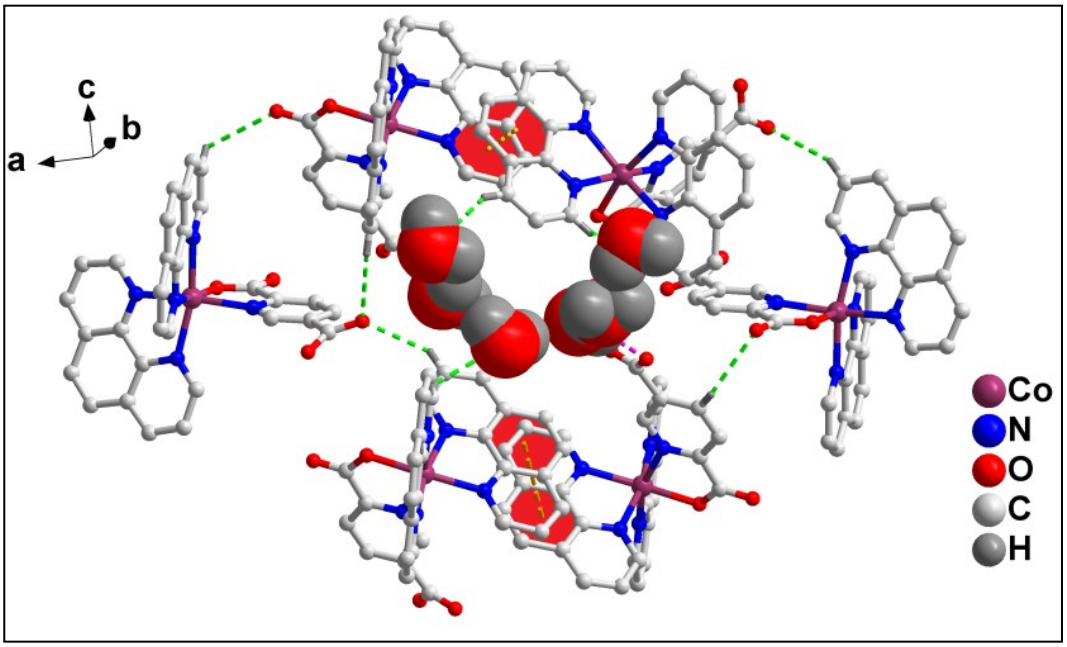

(**b**)

Fig. **S4**(**a**) Formation of linear water cluster in compound **1** involving the lattice water molecules O5, O6, O7, O8; (**b**) Enclathration of the linear water cluster in a hexameric supramolecular host. Irrelevant aromatic hydrogen atoms are omitted for clarity.

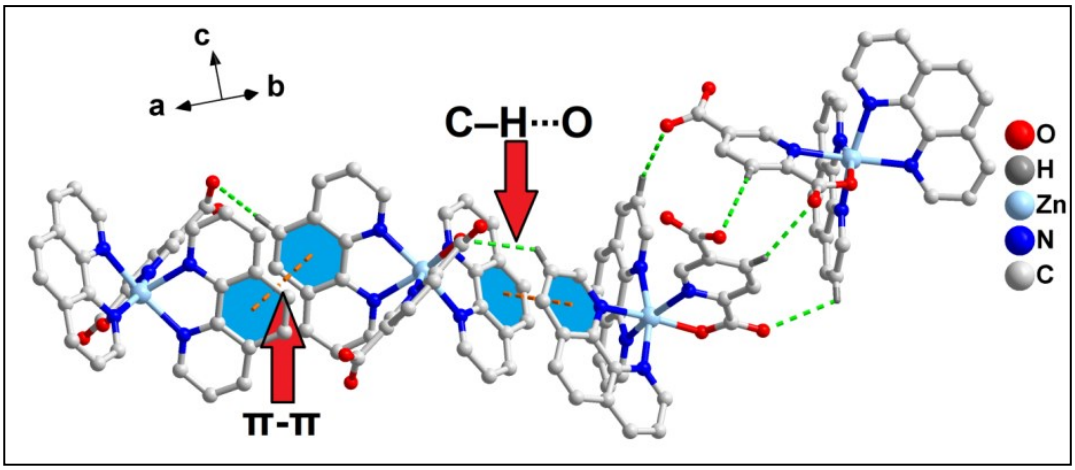

Fig. **S5** 1D supramolecular chain of **2** assisted by non-covalent π-π stacking and C–H···O interactions. Irrelevant aromatic hydrogen atoms are omitted for clarity.

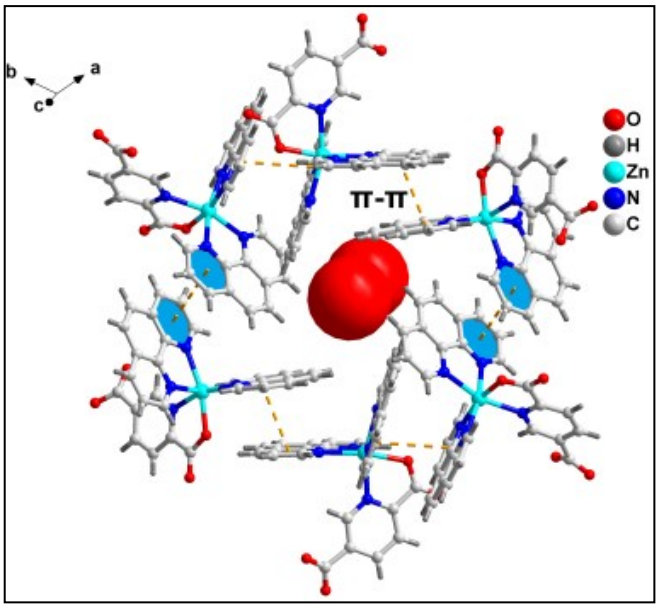

Fig. **S6** Enclathration of dual guest water molecules (O14 and O15) in hexameric supramolecular host of compound **2**.

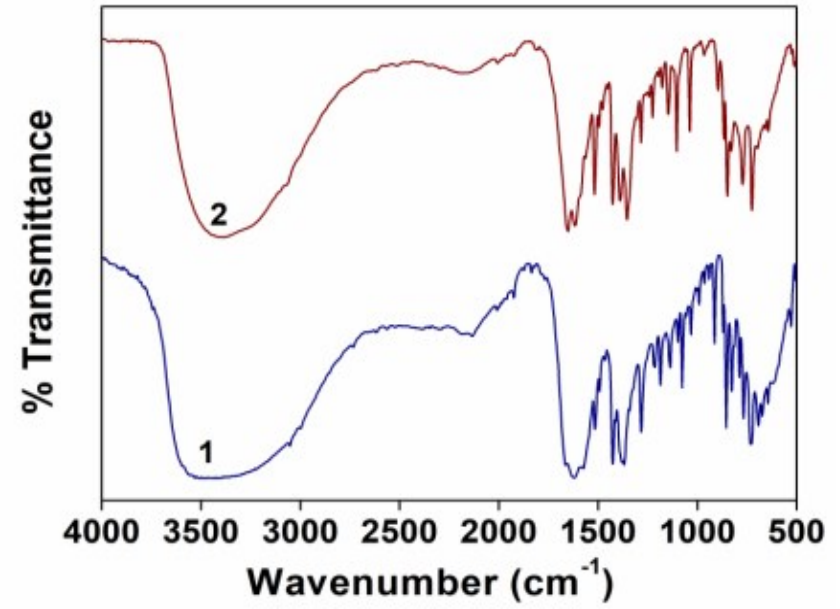

Fig. **S7** FT-IR spectra of compounds **1** and **2**

Electronic spectroscopy

The electronic spectra of compound **1** have been recorded in aqueous as well as in solid phase (Fig. S8). Solid state UV-Vis-NIR spectrum of compound **1** (Fig. S8a) shows absorption peak at around 270 nm assigned to n→π* transitions of the aromatic ligand.[3] For the high-spin octahedral Co(II) complex, we can expect three ligand field bands *viz*. $^4T_{1g}(F)\rightarrow{}^4T_{2g}(F)$ (ν_1), $^4T_{1g}(F)\rightarrow{}^4A_{2g}(F)$ (ν_2) and $^4T_{1g}(F)\rightarrow{}^4T_{1g}(P)$ (ν_3). The first band occurs at 1229 nm, the third band is seen at 509 nm whereas the ν_2 band due to $^4T_{1g}(F)\rightarrow{}^4A_{2g}(F)$ appears at 639 nm.[4] However, the spectrum in water (Fig. S8b) shows weak absorption bands at 495 and 643 nm assigned to $^4T_{1g}(F)\rightarrow{}^4T_{1g}(P)$ (ν_3) and $^4T_{1g}(F)\rightarrow{}^4A_{2g}(F)$ (ν_2) transitions.[5] The NIR band is not seen in the solution spectrum because of the limit in the wavelength window of the spectrophotometer used.[6]

Fig. S9 represents the electronic spectra of compound **2** in solid as well as in aqueous phase. Characteristic absorptions in the solid and aqueous phase spectra at 275 and 274 nm respectively are observed due to π-π* transitions of the aromatic ligands.[7] Absence of spectral band in the visible region for compound **2** in both the phases can be attributed to the d^{10} electronic configuration of the Zn(II) metal centre which does not allow any electronic transition to the higher excited electronic states.[8,9]

The electronic spectral analyses for the compounds **1** and **2** in the solid and in the aqueous solution do not show marked differences and therefore, it may be assumed that the

bonding modes of ligands to the metal centers as well as the geometries of the complexes remains same in both the phases.[10]

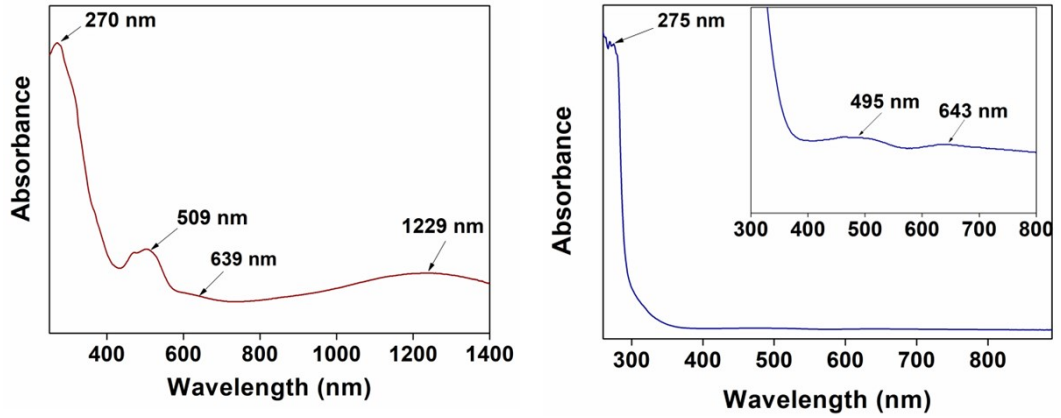

Fig. **S8**(**a**) UV-Vis-NIR spectrum of **1** (**b**) UV-Vis spectrum of **1**

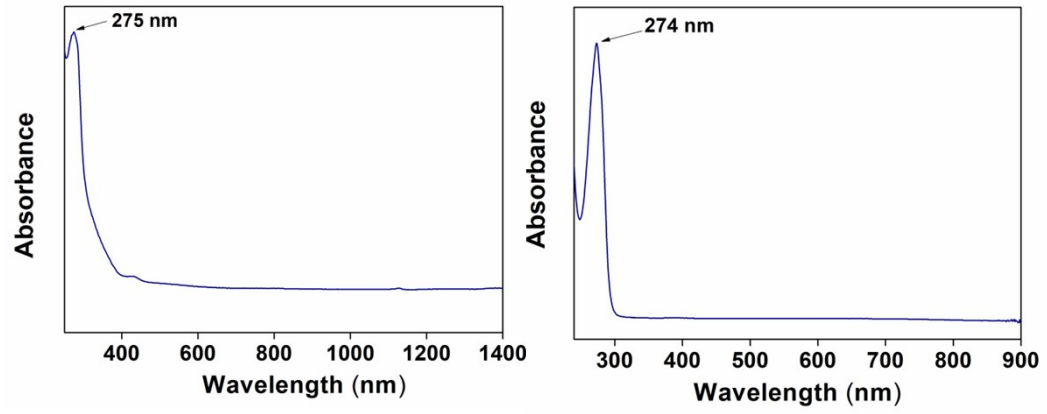

Fig. **S9**(**a**) UV-Vis-NIR spectrum of **2** (**b**) UV-Vis spectrum of **2**

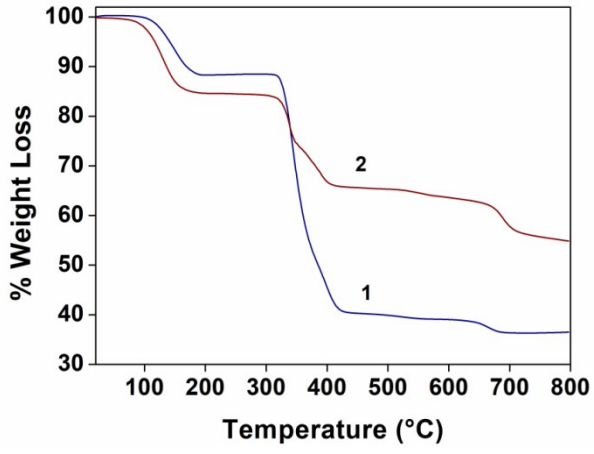

Fig. **S10** Thermogravimetric analyses of compounds **1** and **2**

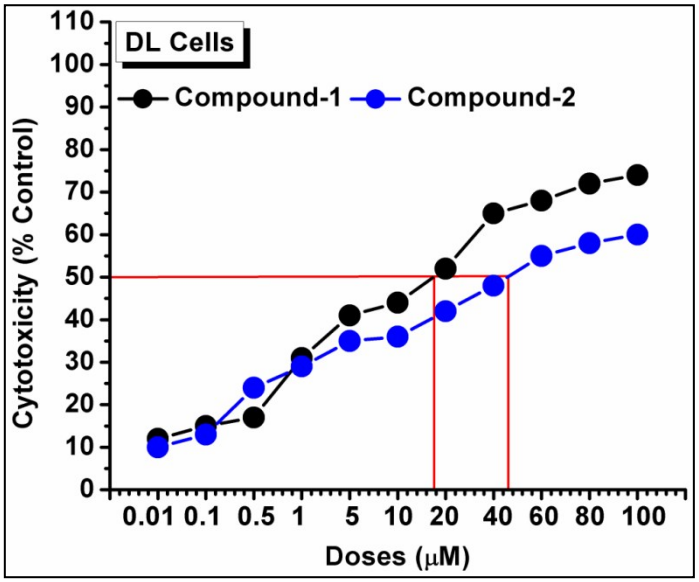

Fig. **S11** IC_{50} plot of compounds **1** and **2** in cancer (DL) cells.

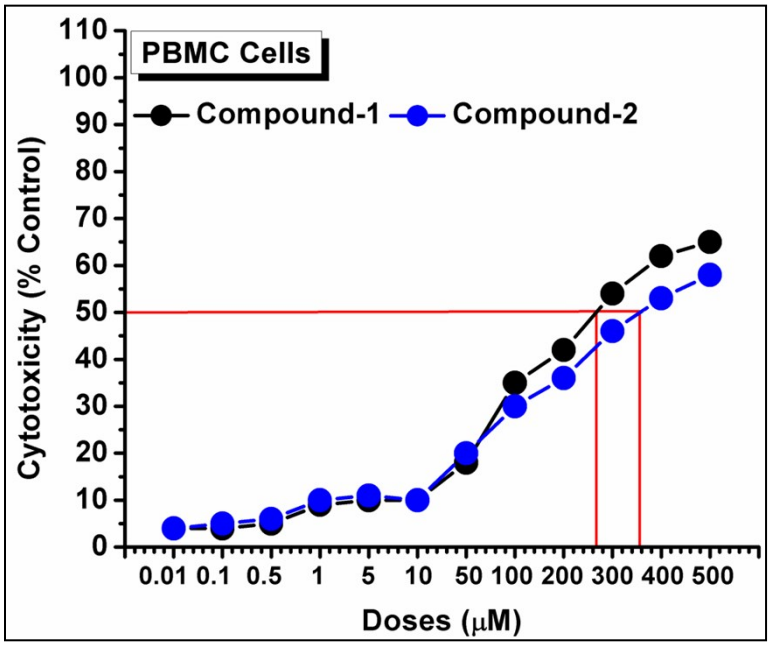

Fig. **S12** IC_{50} plot of compounds **1** and **2** in normal (PBMC) cells.

Table S1 Cell cytotoxicity of compound **1**, compound **2**, *2,5-PDC*, *phen* and metal salts in DL cells. Data represents % cell death as compared to respective untreated control.

Dose (μM)	% Cytotoxicity					
	1	**2**	*phen*	*2,5-PDC*	$CoCl_2 \cdot 6H_2O$	$ZnCl_2$
0	100	100				
0.01	12	10	0	0	0	0

0.1	15	13	0	0	0	0
0.5	17	24	3	4	4	3
1	31	29	4	5	3	4
5	41	35	4	7	5	6
10	44	36	6	8	7	8
20	52	42	8	11	9	10
40	65	48	8	10	11	12
60	68	55	10	12	11	12
80	72	58	12	13	10	14
100	74	60	12	15	13	14
IC_{50}	**17.7**	**46**	**IC_{50} not quantified due to very low cytotoxicity**			

Table S2 Cell cytotoxicity of compound **1**, compound **2**, *2,5-PDC*, *phen* and metal salts in PBMC cells. Data represents % cell death as compared to respective untreated control.

Dose (μM)	% Cytotoxicity					
	1	**2**	*phen*	*2,5-PDC*	$CoCl_2 \cdot 6H_2O$	$ZnCl_2$
0.01	4	4	0	0	0	0
0.1	4	5	0	0	0	0
0.5	5	6	0	0	0	0
1	9	10	0	0	0	0
5	10	11	0	0	0	0
10	10	10	0	0	0	0
50	18	20	3	5	7	4
100	35	30	5	7	7	6
200	42	36	8	9	10	7
300	54	46	10	12	13	8
400	62	53	12	12	15	10
500	65	58	12	14	16	12
IC_{50}	**265**	**356**	**IC_{50} not quantified due to very low cytotoxicity**			

3.9 Pharmacophore modelling

In the current field of drug discovery, pharmacophore modelling is one of the most widely used tool for drug design that led to the establishment of more stable and targeted drugs with no or minimal side effects in the host, as they could be targeted more precisely.[11] The method of determining a target, synthesizing bio-active compounds with desirable pharmacological activities such as minimal toxicity, high bioavailability, cost-effective synthesis, etc. and eventually bringing it to the market is really a time-consuming and expensive endeavour.[12] Ligandscout, a standalone tool, is effectively used in modern drug discovery which solves all the problems associated with the pharmacological activities of the drugs.[13] Pharmacophore functionality may also be used to scan or compare related bioactive molecules based on 3D descriptors with known biological activities from the catalog of the chemical libraries. Important pharmacophore features of the structures of the compounds **1** and **2** have been described here, including hydrophobic, H-bond donor and H-bond acceptor

that may be responsible for the significant biological activities (Fig. S13). It has been observed that the oxygen atoms of the carboxylate groups of the *2,5-PDC* serves as a hydrogen bond acceptor (HBA) and hydrogen bond donor (HBD). The important pharmacophore features of the structure of the compound **1** are: three H-bond donors (HBD), four H-bond acceptors (HBA) and one negatively ionizable (NI) group; whereas, for compound **2**, they are: three H-bond donors (HBD), four H-bond acceptors (HBA), four hydrophobic centers (H) and one positively ionizable (PI) group. In the drug optimization phase, it is also noteworthy that electron withdrawing or donating substituents have opposite effects on the operation of the compounds. Some of the underlying causes of these Structure Activity Relationships (SARs) may be traced to a modulation of the hydrogen-bonding interaction of the inhibitor with the receptor.[14] H-bonds are commonly considered to be protein-ligand binding facilitators.[15] However the introduction of H-bond donors or acceptors to create stronger protein-ligand interactions also results in differential binding affinities.[16]

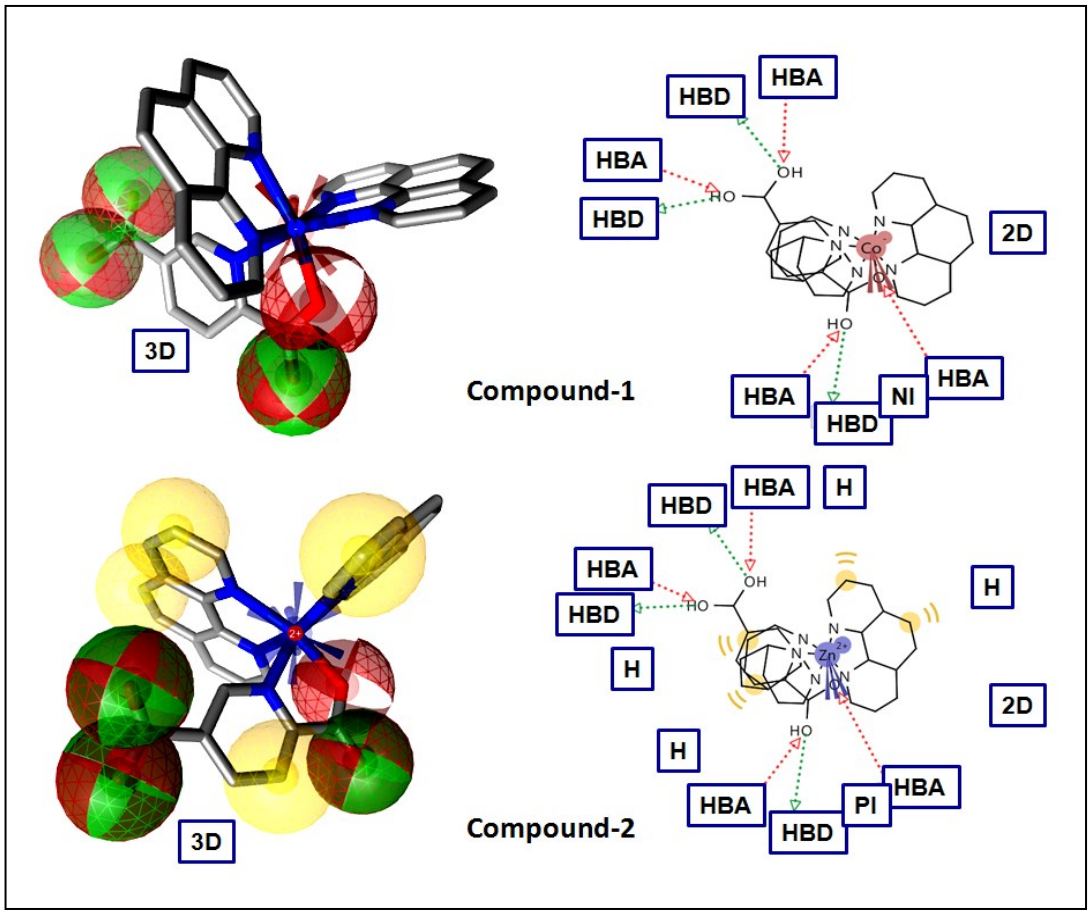

Fig. **S13** Pharmacophore features (2D and 3D) of compounds **1** and **2** predicted using Ligandscout software. Pharmacophore feature includes hydrophobic (H), hydrogen bond donor (HBD), negative ionisable (NI) and hydrogen bond acceptor (HBA).

Suppleentary References

1 A. Gogoi, D. Dutta, A. K. Verma, H. Nath, A. Frontera, A. K. Guha and M. K. Bhattacharyya, *Polyhedron*, 2019, **168**, 113-126.

2 M. A. Al-shaer, Q. A. Al-Balas, M. A. Hassan, G. A. Al-Jabal and A. M. Almaaytah, *Comput. Biol. Chem*., 2019, **80**, 102-110.

3 U. Saha, D. Dutta, A. Bauzá, A. Frontera, B. Sarma and M. K. Bhattacharyya, *Polyhedron*, 2019, **159**, 387-399.

4 (a) S. M. N. Islam, D. Dutta, A. K. Guha and M. K. Bhattacharyya, *J. Mol. Struct*., 2019, **1175**, 130-138;

(b) D. Dutta, S. M. N. Islam, U. Saha, A. Frontera and M. K. Bhattacharyya, *J. Mol. Struct.*, 2019, **1195**, 733-743.

5 S. J. Bora and B. K. Das, *J. Solid State Chem*., 2012, **192**, 93-101.

6 D. Dogan, A. T. Colak, O. Sahin, T. Tunc and O. Celik, *Polyhedron*, 2015, **93**, 37-45.

7 C. S. Zhang, J. Li, K. L. Hou, Y. H. Xing and Z. Shi, *Spectrochim. Acta*, 2011, **78**, 777-782.

8 (a) S. M. N. Islam, D. Dutta, A. K. Verma, H. Nath, A. Frontera, P. Sharma and M. K. Bhattacharyya, *Inorg. Chim. Acta*, 2019, **498**, 119161-119174;

(b) D. Dutta, S. M. N. Islam, U. Saha, S. Chetry, A. K. Guha and M. K. Bhattacharyya, *J. Chem. Cryst*., 2018, **48**, 156-163.

9 M. K. Bhattacharyya, U. Saha, D. Dutta, A. Frontera, A. K. Verma, P. Sharma and A. Das, *New J. Chem*., 2020, **44**, 4504-4518.

10 (a) M. Ghosh, A. Majee, M. Nethaji and T. Chattopadhyay, *Inorg. Chim. Acta*, 2009, **362**, 2052-2055;

(b) P. Sharma, A. Gogoi, A. K. Verma, A. Frontera and M. K. Bhattacharyya, *New J. Chem*., 2020, **44**, 5473-5488.

11 A. Daina, O. Michielin and V. Zoete, *Sci. Rep.*, 2017, **7**, 1-13.

12 P. Muntha, *J. Pharm. Pharm. Sci*., 2016, **5**(**1**), 135-142.

13 G. Wolber and R. Kosara, *Methods and Principles in Medicinal Chemistry*, 2006, **32**, 131-150.

14 A. H. Bingham, R. J. Davenport, L. Gowers, R. L. Knight, C. Lowe, D. A. Owen, D. M. Parry and W. R. Pitt, *Bioorg. Med. Chem. Lett*., 2004, **14**(**5**), 409-412.

15 S. Salentin, V. J. Haupt, S. Daminelli and M. Schroeder, *Prog. Biophys. Mol. Biol*., 2014, **116**, 174-186.

16 V. Lafont, A. A. Armstrong, H. Ohtaka, Y. Kiso, L. M. Amzel and E. Freire, *Chem. Biol. Drug Des*., 2007, **69**(**6**), 413-422.